Available online at www.sciencedirect.com
SCIENCE DIRECT®
Journal of Computational Physics 188 (2003) 209–231
JOURNAL OF COMPUTATIONAL PHYSICS
www.elsevier.com/locate/jcp

High accuracy periodic solutions to the Sivashinsky equation ☆

V. Karlin [a,*], V. Maz'ya [b], G. Schmidt [c]

[a] Centre for Research in Fire and Explosions, University of Central Lancashire, Preston PR1 2HE, UK
[b] Department of Mathematics, Linköping University, Linköping S-581 83, Sweden
[c] Weierstrass Institute for Applied Analysis and Stochastics, Mohrenstrasse 39, Berlin D-10117, Germany

Received 29 May 2001; received in revised form 20 October 2002; accepted 3 March 2003

Abstract

The aim of this work is the accurate calculation of periodic solutions to the Sivashinsky equation, which models dynamics of the long wave instability of laminar premixed flame. A highly accurate computational algorithm was developed in both one and two spatial dimensions and its crucial implementation details are presented. The algorithm is based on the concept of saturated asymptotic approximations and can be straightforwardly extended to a wide variety of nonlinear integro-differential equations. The development of such an algorithm was motivated by difficulties in interpretation of the results of numerical experiments with the Sivashinsky equation using spectral methods. The computations carried out by the algorithm in question are in good agreement with the results obtained earlier by spectral methods. Analysis of the accuracy of obtained numerical solutions and of their stabilization to steady states supports the idea of the instability of the steady coalescent pole solutions (with maximal possible number of poles) to the Sivashinsky equation in large domains through huge linear transient amplification of nonmodal perturbations of small but finite amplitudes.

1. Introduction

Sivashinsky's equation was obtained in [24] as a weakly nonlinear long wave asymptotic of the Navier–Stokes system combined with the infinite activation energy model of premixed combustion chemistry. The equation governs evolution of the perturbation $\Phi(x_1, x_2, t)$ of the plane flame front moving in the x_3-direction with the laminar flame speed u_b. Thus, at a given instant of time t, the surface of the flame front is described as $x_3 = t + \Phi(x_1, x_2, t)$, where space coordinates are measured in units of the flame front width δ_{th} and time is in units of δ_{th}/u_b. In these notations, the Sivashinsky equation can be written as follows:

☆ Research supported by EPSRC Grants GR/K95932 and GR/R66692.
* Corresponding author.
E-mail addresses: VKarlin@uclan.ac.uk (V. Karlin), vlmaz@math.liu.se (V. Maz'ya), schmidt@wias-berlin.de (G. Schmidt).

0021-9991/03/$ - see front matter
doi:10.1016/S0021-9991(03)00164-5

$$\frac{\partial \Phi}{\partial t} - \frac{1}{2}\left[\left(\frac{\partial \Phi}{\partial x_1}\right)^2 + \left(\frac{\partial \Phi}{\partial x_2}\right)^2\right] = \frac{\partial^2 \Phi}{\partial x_1^2} + \frac{\partial^2 \Phi}{\partial x_2^2} - \frac{\gamma}{4\pi}\left(\frac{\partial^2}{\partial x_1^2} + \frac{\partial^2}{\partial x_2^2}\right)\int_{\mathbb{R}^2} \frac{\Phi(y_1, y_2, t)\,\mathrm{d}y_1\,\mathrm{d}y_2}{\sqrt{(x_1 - y_1)^2 + (x_2 - y_2)^2}},$$
$$(x_1, x_2) \in \mathbb{R}^2. \tag{1}$$

In the derivation of (1) the wavelengths of the perturbations were assumed to be much greater than the width of the flame front. Hence, the flame front was considered as a surface separating a combustible mixture of density ρ_u and burnt gases of density ρ_b. An assumption of low expansion rate $\rho_b/\rho_u \approx 1$ was also used in order to justify the appearance of the nonlinearity in (1), where the parameter $\gamma = 1 - \rho_b/\rho_u$. Eventually, its weak nonlinearity means that $|\nabla \Phi|$ is assumed to be small.

Because of the asymptotic origins of (1), see [25], it cannot be used to model thermal-diffusive instabilities which may occur for sufficiently small values of the Lewis number. The proper model to treat this kind of instabilities was also obtained in [24] and is called the Kuramoto–Sivashinsky equation.

Physically, (1) governs uniform propagation of the flame front along the normal to its surface with the speed u_b affected by the Landau–Darrieus instability [12,14]. Eq. (1) can be written as $\Phi_t - 2^{-1}|\nabla \Phi|^2 = \Delta \Phi + 2^{-1}\gamma(-\Delta)^{1/2}\Phi$ and is reduced in one dimension to

$$\frac{\partial \Phi}{\partial t} - \frac{1}{2}\left(\frac{\partial \Phi}{\partial x}\right)^2 = \frac{\partial^2 \Phi}{\partial x^2} + \frac{\gamma}{2}\frac{\partial \mathscr{H}[\Phi]}{\partial x}, \quad x \in \mathbb{R}, \tag{2}$$

where $\mathscr{H}[\Phi]$ is the Hilbert transform. Note, that if $\Phi_1(x,t)$ is a Λ_1-periodic solution to (2) for $\gamma = \gamma_1$, then

$$\Phi_2(x,t) = \Phi_1[(\Lambda_1/\Lambda_2)x, (\gamma_2\Lambda_1/\gamma_1\Lambda_2)t] \tag{3}$$

is a Λ_2-periodic solution to (2) for $\gamma = \gamma_2$ if $\gamma_1\Lambda_1 = \gamma_2\Lambda_2$. This gives a reason to study (1) for any γ, though proper scaling maybe required in order to interpret obtained results from the physical point of view.

A wide class of periodic solutions to (2) was obtained in [26] by using the pole decomposition technique. Namely, it was shown that

$$\Phi(x,t) = 2\pi N_\mathrm{p}\Lambda^{-1}(\gamma - 4\pi N_\mathrm{p}\Lambda^{-1})t + 2\sum_{n=1}^{N_\mathrm{p}} \ln\left|\cosh\left[2\pi\Lambda^{-1}b_n(t)\right] - \cos\left\{2\pi\Lambda^{-1}[x - a_n(t)]\right\}\right| \tag{4}$$

is a Λ-periodic solution to (2) if $a_n(t)$, $b_n(t)$, $n = 1, \ldots, N_\mathrm{p}$, satisfy a system of ODE's, which is available elsewhere and is known as the pole dynamics system. Here N_p is an arbitrary positive integer.

At any time instant t complex numbers $z_n(t) = a_n(t) \pm \mathrm{i}b_n(t)$, $n = 1, \ldots, N_\mathrm{p}$ are poles of (4). Correspondingly, (4) is called the N_p-pole solution of (2). If all the poles are steady and $a_n = a \in \mathbb{R}$ for $n = 1, \ldots, N_\mathrm{p}$, then (4) is called a steady coalescent N_p-pole solution. Solutions of the latter type are denoted here as $\Phi_{N_\mathrm{p}}(x)$. It was shown, see for example [23], that for a given period Λ the number of poles in the steady coalescent pole solution (4) may not exceed $N_{\mathrm{p},\Lambda} = \mathrm{ceil}(\gamma\Lambda/8\pi + 1/2) - 1$, where $\mathrm{ceil}(x)$ is the smallest integer greater or equal to x.

Computational studies of (2) are usually undertaken in a finite domain of large enough size L assuming the L-periodicity of the solutions. The eigenvalue analysis of (2) linearized on the steady coalescent pole solutions of the period Λ commensurable with L was carried out both numerically [19] and analytically [29]. The analysis indicated that for any $L > 0$ the steady coalescent $N_{\mathrm{p},L}$-pole solution is the only steady coalescent N_p-pole solution to (2) with no eigenvalues located to the right from the imaginary axis. Accordingly, direct numerical experiments revealed that for sufficiently small values of $L < L_\mathrm{c}$ numerical solutions converge to $\Phi_{N_{\mathrm{p},L}}(x,t)$. However, for larger computational domains $L > L_\mathrm{c}$, numerical solutions to (2) do not stabilize to any steady solution at all. Instead, being essentially nonsteady, they remain very closely to the steady coalescent $N_{\mathrm{p},L}$-pole solution, developing on the surface of the flame front small cusps arbitrary

in time and space [23]. With time these small cusps move towards the trough of the flame front profile and disappear in it as this is shown in Fig. 1.

Even if the spectrum of the linearized problem is located entirely in the left half of the complex plane there is still a variety of possible reasons for numerical solutions not to converge to $\Phi_{N_{p,L}}(x,t)$ for large enough L. For example, the high sensitivity of pole solutions to certain perturbations of small but finite amplitudes was suggested in [8] as an explanation of the cardinal change in the behaviour of numerical solutions to (2) which takes place for $L = L_c$. The argument of [8] was based on a particular asymptotic solution of an approximation to the Sivashinsky equation linearized on the steady coalescent $N_{p,L}$-pole solution. That solution exhibits a very strong transient growth during which the energy of the perturbation is amplified of order $e^{O(L)}$ times. Similar conclusions on high sensitivity of the Sivashinsky equation to noise were made in [19]. In the Hagen–Poiseuille flow such sensitivity to noise was shown to be the reason of the subcritical transition to turbulence, see [2,6].

In computer simulations both approximation residuals and round-off errors can be considered as finite amplitude perturbations or noise and for this reason deserve a special investigation. Sometimes both of them are united and referred to as "numerical artefacts." However, the answer to the question which of them is the reason of not stabilization of solutions to (2) for $L > L_c$ would have contrasting implications for the physical status of the Sivashinsky equation. Investigation of the numerical aspects of solving of the Sivashinsky equation as a possible reason of not stabilization of its numerical solutions for $L > L_c$ is the primary physical objective of this work.

Taking into account that most of previous numerical studies of (2), see, e.g. [4,5,7,18,19,22,23] were based on spectral methods, it is reasonable to try an essentially different approach with a dissimilar approximation residual. An obvious alternative is the method of finite differences whose main advantage is simplicity. However, numerical investigation of stability of steady coalescent $N_{p,L}$-pole solutions of (2) requires a highly accurate computational algorithm and attempts to develop high order finite-difference approximations of (1) and (2) result in quite cumbersome formulas. Most of troubles come from the integral term with the singularity in the kernel.

In this work we develop an algorithm based on saturated asymptotic approximations, which are known also as "approximate approximations" [15]. The order of approximation of the saturated asymptotic approximations is controlled by an explicit parameter and theoretically achievable accuracy of the approximation is limited by the smoothness of approximated solutions only. This gives us a reason to claim that theoretically the saturated asymptotic approximations are as accurate as the spectral method. Further, the

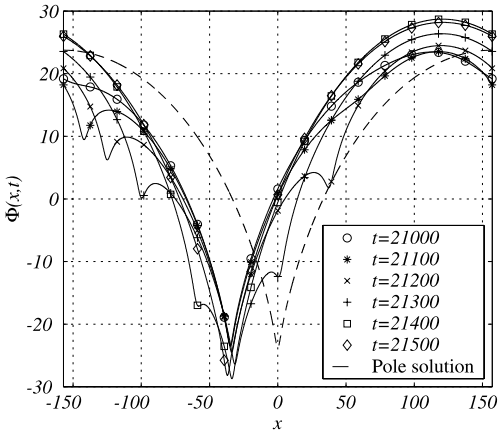

Fig. 1. Appearance of small cusps on the surface of the flame front for $\gamma = 0.8$ and $L = 100\pi$. Corresponding solution $\Phi_{N_{p,L}}(x,t)$ is also given. Here $N_{p,L} = 10$.

computational formulas of the algorithm are uniform in regard to the parameter of the order of the approximation and, unlike to the method of finite differences, their complexity does not grow with that parameter. Thus, for low orders of approximation the proposed method may look more complicated than the finite-differences, but for highly accurate calculations this is no longer obvious. The last but not least is that similarly to the finite differences and in contrast to the spectral approximations, the accuracy of the saturated asymptotic approximations is only degraded locally if the smoothness of the approximated function is lost locally. The latter property of the method can be especially beneficial for bifurcating solutions with smoothness degrading at the moments of bifurcations. The algorithm in question was proved to be efficient for nonlocal problems in infinite domains [9,10] and is extended here to tackle periodic solutions.

The method of saturated asymptotic approximations provides high order approximations of sufficiently smooth functions up to certain prescribed accuracy. Consider for example the approximation of $g(x)$ by the formula

$$g(x) \approx g_h(x) = \frac{1}{\sqrt{D}} \sum_{m=-\infty}^{\infty} g_m \eta_{\mathcal{N}}\left(\frac{x - mh}{\sqrt{D}h}\right), \quad x \in \mathbb{R}. \tag{5}$$

with $g_m = g(hm)$. Here $\eta_{\mathcal{N}}(x)$ is a smooth and rapidly decaying basis function, satisfying the moment condition

$$\int_{-\infty}^{\infty} \eta_{\mathcal{N}}(x)\,\mathrm{d}x = 1, \quad \int_{-\infty}^{\infty} x^n \eta_{\mathcal{N}}(x)\,\mathrm{d}x = 0, \quad n = 1, \ldots, \mathcal{N} - 1.$$

Then for any $\varepsilon > 0$ there exists $D > 0$ that

$$|g(x) - g_h(x)| \leqslant c_\eta (\sqrt{D}h)^{\mathcal{N}} \|g^{(\mathcal{N})}\|_{L_\infty} + \varepsilon \sum_{n=0}^{\mathcal{N}-1} (\sqrt{D}h)^n |g^{(n)}(x)|$$

(cf. [16]). An example of a suitable basis function is given by

$$\eta_{\mathcal{N}}(x) = \eta_{2N+2}(x) = e_N\left(-\frac{1}{4}\frac{\mathrm{d}^2}{\mathrm{d}x^2}\right)\frac{\mathrm{e}^{-x^2}}{\sqrt{\pi}} = \frac{(-1)^N \mathrm{e}^{-x^2}}{\sqrt{\pi}\, 2^{2N+1} N!}\,\frac{\mathrm{H}_{2N+1}(x)}{x}, \tag{6}$$

where $e_N(x) = \sum_{k=0}^{N} x^k/k!$ is the truncated exponent function, and $\mathrm{H}_n(x)$ denotes the Hermite polynomial of order n. The function (6) is not a unique possible basis, but just a choice of many others [17]. Note that formula (5) allows straightforward generalizations to the multivariate case.

Formula (5) with (6) provides approximation of order $\mathrm{O}(h^{2N+2})$ plus a small saturation term $\varepsilon = \mathrm{O}(\mathrm{e}^{-\pi^2 D})$, see [15]. This term does not disappear when $h \to 0$, instead it vanishes as $D \to \infty$. In particular, it can be made less than machine zero ε_M of the computer used in calculations, and, normally, does not produce errors greater than the machine zero does. The accuracy of the saturated asymptotic approximations (5), (6) is limited only by the smoothness of approximated solutions and by the number of the vanishing moments of the basis function.

Smoothing properties of Gaussians were intensively exploited earlier, for example, in the grid-free vortex methods for the incompressible fluid dynamics equations, see, e.g. [13] and references therein. However, the grid based approximations (5) were first introduced in [15] and studied, for example, in [16,17].

In Section 2 we develop the algorithm for Sivashinsky's equation in one spatial dimension, and, in Section 3, the algorithm is extended to the two-dimensional case. In Section 4 we present results of numerical simulations for both one- and two-dimensional Eqs. (1) and (2). These computations indicate that the non-stabilization of numerical solutions in large enough computational domains is of numerical origins and that the small cusps appearing on the flame surface for $L > L_c$ are generated by the round-off errors. Conclusions are given in Section 5.

2. Computational algorithm in one dimension

2.1. Discretization in time

We approximate the one-dimensional equation (2) in time as follows:

$$\frac{\Phi^{(n+1)}-\Phi^{(n)}}{\Delta t}=\sigma_1\mathscr{L}\Phi^{(n+1)}+(1-\sigma_1)\mathscr{L}\Phi^{(n)}+\frac{\sigma_1}{2}\left(\frac{\partial\Phi}{\partial x}\right)^2_{t=t_{n+1}}+\frac{\sigma_2}{2}\left(\frac{\partial\Phi}{\partial x}\right)^2_{t=t_n}+\frac{1-\sigma_1-\sigma_2}{2}\left(\frac{\partial\Phi}{\partial x}\right)^2_{t=t_{n-1}}. \tag{7}$$

Here $\mathscr{L}$ is the pseudodifferential operator composed of linear terms of the Sivashinsky equation

$$\mathscr{L}\Phi=\frac{\partial^2\Phi}{\partial x^2}+\frac{\gamma}{2}\frac{\partial\mathscr{H}[\Phi]}{\partial x}, \tag{8}$$

and $\Phi^{(n)}=\Phi(x,n\Delta t)$, $n=0,1,\ldots$ The three time-layer interpolation of the nonlinear term provides a possibility to obtain approximations of second order explicitly. Variable time steps can be used in (7) as well subject to proper modification of the time interpolation in the right-hand side. Unlike the variety of available choices for weight coefficients, two major cases of (7) with $\sigma_I=\sigma_1=\sigma_2=1/2$, and $\sigma_I=1/2$, $\sigma_1=0$, $\sigma_2=3/4$ were tested in practice.

Linearizing $(\partial\Phi/\partial x)^2_{t=t_{n+1}}$ in (7) with respect to $\Delta\Phi=\Phi^{(n+1)}-\Phi^{(n)}$ for $\Phi=\Phi^{(n)}$ and factorizing the implicit operator, one obtains

$$(I-\Delta t\sigma_I\mathscr{L})\left[I-\Delta t\sigma_1\frac{\partial\Phi^{(n)}}{\partial x}\frac{\partial}{\partial x}\right]\frac{\Phi^{(n+1)}-\Phi^{(n)}}{\Delta t}=\mathscr{L}\Phi^{(n)}+G^{(n)},$$

where

$$G^{(n)}=\frac{\sigma_1+\sigma_2}{2}\left(\frac{\partial\Phi}{\partial x}\right)^2_{t=t_n}+\frac{1-\sigma_1-\sigma_2}{2}\left(\frac{\partial\Phi}{\partial x}\right)^2_{t=t_{n-1}}, \tag{9}$$

and I is the identity operator. Alternatively, Eq. (7) could be split into fractional time steps.

The factorized equation is solved in two stages, first relatively to $Y^{(n)}$:

$$(I-\Delta t\sigma_I\mathscr{L})Y^{(n)}=\mathscr{L}\Phi^{(n)}+G^{(n)}, \tag{10}$$

and then relatively to $(\Phi^{(n+1)}-\Phi^{(n)})/\Delta t$:

$$\left[I-\Delta t\sigma_1\frac{\partial\Phi^{(n)}}{\partial x}\frac{\partial}{\partial x}\right]\frac{\Phi^{(n+1)}-\Phi^{(n)}}{\Delta t}=Y^{(n)}. \tag{11}$$

With $\partial\Phi^{(n)}/\partial x$ and $\partial/\partial x$ approximated by finite differences, the solution of (11) is straightforward, if $\sigma_1\neq 0$ and is not required at all otherwise. For example, forward and backward sweeps of LU decomposition can be used. The operator $\partial/\partial x$ in (11) has been approximated by the central finite-differences of the second order. However, the central finite-difference approximations of up to the 8th order were tested for spatial derivatives $\partial\Phi/\partial x$ in (9) and (11).

In terms of the Fourier transform $\mathscr{F}[f](\xi)=\int_{-\infty}^{\infty}f(x)\mathrm{e}^{-\mathrm{i}2\pi\xi x}\,\mathrm{d}x$ the solution to (10) can be written as follows

$$Y^{(n)}(x) = (I - \Delta t\sigma_I \mathscr{L})^{-1}(\mathscr{L}\Phi^{(n)} + G^{(n)}) = \int_{-\infty}^{\infty} \frac{\mathscr{F}[\mathscr{L}](\xi)\mathscr{F}[\Phi^{(n)}](\xi) + \mathscr{F}[G^{(n)}](\xi)}{1 - \Delta t\sigma_I \mathscr{F}[\mathscr{L}](\xi)} \mathrm{e}^{\mathrm{i}2\pi\xi x}\,\mathrm{d}\xi, \tag{12}$$

where $\mathscr{F}[\mathscr{L}](\xi) = -4\pi^2\xi^2 + \pi\gamma|\xi|$ is the Fourier image of (8). The evaluation of the Fourier integral (12) is one of the major components of the computational algorithm in question.

2.2. Inversion of the integral operator

A standard way of calculating the Fourier transform and, eventually, the integral (12), is to approximate the integrand by a series expansion with respect to a set of relatively simple basis functions. Then, the calculation of the Fourier transform of an arbitrary function will be reduced to the evaluation of the Fourier images of the basis functions. In sequel, the calculation of the value of the operator $(I - \Delta t\sigma_I \mathscr{L})^{-1}$ on $\mathscr{L}\Phi^{(n)} + G^{(n)}$, for arbitrary functions $\Phi^{(n)}$ and $G^{(n)}$, will be reduced to evaluating its values on the basis functions. In this work saturated asymptotic approximations are used in order to approximate $\Phi^{(n)}(x)$ and $G^{(n)}(x)$.

It is easy to see that expansion (5), (6) preserves parity of the approximated function. Indeed, if $g(-x) = \pm g(x)$, $x \in \boldsymbol{R}$, then $g_h(-x) = \sum_{m=-\infty}^{\infty} g_m \eta_{\mathscr{N}}(-x - mh) = \sum_{m=-\infty}^{\infty} g_m \eta_{\mathscr{N}}(x + mh)$, because $\eta_{\mathscr{N}}(x)$ from (6) is an even function. By introducing a new index $n = -m$, we have $g_h(-x) = \sum_{n=\infty}^{-\infty} g_{-n}\eta_{\mathscr{N}}(x - nh) = \pm\sum_{n=-\infty}^{\infty} g_n \eta_{\mathscr{N}}(x - nh)$, or $g_h(-x) = \pm g_h(x)$.

Also, saturated asymptotic approximations (5) retain periodicity of the approximated function if the period $X \in \mathbb{R}$ is commensurable with the parameter of approximation h. One may write $g_h(x + X) = \sum_{m=-\infty}^{\infty} g_m \eta_{\mathscr{N}}(x + X - mh) = \sum_{m=-\infty}^{\infty} g_m \eta_{\mathscr{N}}[x - (mh - X)]$. Assuming that $X/h = M_X$ is an integer and introducing a new index $n = m - M_X$, we have $g_h(x + X) = \sum_{n=-\infty}^{\infty} g_{n+M_X}\eta_{\mathscr{N}}(x - nh) = \sum_{n=-\infty}^{\infty} g_n \eta_{\mathscr{N}}(x - nh)$, because $g_{n+M_X} = g(nh + M_X h) = g(nh + X) = g(nh) = g_n$. Thus $g_h(x + X) = g_h(x)$ for $X/h \in \mathbb{Z}$.

Application of the Fourier transform to (5), (6) yields

$$\mathscr{F}[g](\xi) \approx \mathscr{F}[g_h](\xi) = \sum_{m=-\infty}^{\infty} g_m \mathscr{F}[\eta_{\mathscr{N}}(x - mh)](\xi), \tag{13}$$

where $\mathscr{F}[\eta_{\mathscr{N}}(x - mh)](\xi) = he_N(\pi^2 Dh^2\xi^2)\mathrm{e}^{-\pi^2 Dh^2\xi^2 - \mathrm{i}2\pi mh\xi}$. Use of (13) in (12) results in the convolution

$$Y_k^{(n)} = \sum_{m=-\infty}^{\infty} C_{k-m}^{(1)} \Phi_m^{(n)} + C_{k-m}^{(2)} G_m^{(n)}, \quad k \in \mathbb{Z}, \tag{14}$$

where the coefficients are given by the Fourier integral

$$C_l^{(j)} = 2h \int_0^{\infty} F_j(\xi)\cos 2\pi hl\xi\,\mathrm{d}\xi, \quad j = 1, 2, \ \ l \in \mathbb{Z}, \tag{15}$$

with

$$F_1(\xi) = \mathscr{F}[\mathscr{L}](\xi)F_2(\xi), \quad F_2(\xi) = \frac{e_N(\pi^2 Dh^2\xi^2)\mathrm{e}^{-\pi^2 Dh^2\xi^2}}{1 - \Delta t\sigma_I \mathscr{F}[\mathscr{L}](\xi)}. \tag{16}$$

Note, that $C_l^{(1)} = (\sigma_I \Delta t)^{-1}[C_l^{(2)} - \eta_{\mathscr{N}}(lh)]$ for $l \in \mathbb{Z}$, and the following parity symmetries are held:

$$C_{-l}^{(j)} = C_l^{(j)}, \quad j = 1, 2, \ \ l \in \mathbb{Z}. \tag{17}$$

Considering space periodic solutions and assuming that their period L is commensurable with the discretization parameter h, i.e., $L/h = 2M \in \mathbb{Z}$, we have $\Phi_m^{(n)} = \Phi_{m+2M}^{(n)}$, $G_m^{(n)} = G_{m+2M}^{(n)}$ for $m \in \mathbb{Z}$. Here, use of an

even number for L/h is not a restriction. All the following results take place for odd values of L/h either, but formulas and programming are more complex.

Assuming L-periodicity, formula (14) can be transformed into

$$Y_k = \sum_{m=k-M}^{k+M-1} B_{k-m}^{(1,M)} \Phi_m^{(n)} + B_{k-m}^{(2,M)} G_m^{(n)}, \quad k = -M, \ldots, M-1, \tag{18}$$

where

$$B_l^{(j,M)} = C_l^{(j)} + \sum_{\mu=1}^{\infty} \left(C_{2\mu M+l}^{(j)} + C_{2\mu M-l}^{(j)} \right), \quad j = 1,2, \;\; l = -M+1, \ldots, M, \tag{19}$$

because of (17). Functions $\Phi_m^{(n)}$ and $G_m^{(n)}$ are involved in (18) for $m = -2M, \ldots, 2M-2$.

By proper extension of the convolution coefficients $B_l^{(j,M)}$ the sum (18) can be transformed into the discrete circular convolution and calculated by using FFT, see [28].

2.3. Convolution coefficients

The integrands in (15) depend on l through $\cos 2\pi h l \xi$ only. Therefore, after substitution of $C_l^{(j)}$ into (19), a temptation to swap integration and summation may appear. However, the sum

$$\sum_{l=-l_\infty}^{l_\infty} \cos 2\pi h(m-2lM)\xi = \cos 2\pi h m \xi \left[2 \frac{\sin 2\pi h (2l_\infty + 1) M \xi}{\sin 2\pi h M \xi} - 1 \right]$$

does not converge as $l_\infty \to \infty$ and swapping of integration and summation in (19) with (15) is not legal. The discrete Fourier transform is finite and can be swapped with both summation in (19) and integration in (15), but this neither eases (19) nor brings any other benefits.

A better way to tackle the summation in (19) is to use asymptotic expansions of the integral (15). The Laplace method of asymptotic approximation of the integral (15) with even functions (16) rapidly decaying for $\xi \to \infty$, yields

$$C_l^{(j)} = 2h \sum_{\kappa=1}^{K_j} \frac{(-1)^\kappa F_j^{(2\kappa-1)}(0)}{(2\pi h l)^{2\kappa}} + \mathrm{O}\left[\frac{2h\Delta t F_j^{(2K_j+1)}(0)}{(2\pi h l)^{2K_j+2}} \right], \quad j = 1,2, \tag{20}$$

where $F_j^{(\kappa)}(0)$ stands for the κth derivative of $F_j(\xi)$ for $\xi = 0$.

Splitting the summation in (19) as follows:

$$B_l^{(j,M)} = C_l^{(j)} + \sum_{\mu=-\infty}^{-1} C_{l-2\mu M}^{(j)} + \sum_{\mu=1}^{\infty} C_{l-2\mu M}^{(j)}, \quad j = 1,2,$$

and substituting asymptotic expansions (20) results in

$$\begin{aligned} B_l^{(j,M)} = {} & C_l^{(j)} + 2h \sum_{\kappa=1}^{K_j} \frac{(-1)^\kappa F_j^{(2\kappa-1)}(0)}{(4\pi h M)^{2\kappa}} \sum_{\mu=1}^{\infty} \left[\left(\mu + \frac{l}{2M} \right)^{-2\kappa} + \left(\mu - \frac{l}{2M} \right)^{-2\kappa} \right] \\ & + \mathrm{O}\left\{ \frac{2h F_j^{(2K_j+1)}(0)}{(2\pi h)^{2K_j+2}} \sum_{\mu \in \mathbb{Z}\setminus\{0\}} \frac{1}{(l-2\mu M)^{2K_j+2}} \right\}. \end{aligned} \tag{21}$$

The residual of the inner series in (21) cut off at $\mu = M_\infty$ is of order $M_\infty^{-2\kappa+1}$. This means, in turn, that for $\kappa = 1$ direct summation with accuracy of order 10^{-16} would require to take into account about 10^{16} terms and is practically impossible. In order to reduce the computational costs, we represent the summation in terms of the polygamma functions $\psi^{(\kappa)}(x)$ for $l \neq 0$. Further, using the $(2\kappa-1)$th derivative of the symmetry relationship $\psi(x) - \psi(-x) = -\pi\cot\pi x - x^{-1}$, see p. 774 in [20], together with the representation of $\alpha^{-2\kappa}$ as the $(2\kappa-1)$th derivative of α^{-1}, yields the required formula:

$$B_l^{(j,M)} = C_l^{(j)} + 2h\sum_{\kappa=1}^{K_j} \frac{(-1)^{\kappa-1}F_j^{(2\kappa-1)}(0)}{(4hM)^{2\kappa}(2\kappa-1)!} \left.\frac{\mathrm{d}^{2\kappa-1}(\cot\alpha - \alpha^{-1})}{\mathrm{d}\alpha^{2\kappa-1}}\right|_{\alpha=\pi|l|/2M} + \mathrm{O}\left[\frac{6hF_j^{(2K_j+1)}(0)}{(2\pi hM)^{2K_j+2}}\right],$$
$$l = -M+1,\ldots,-1,1,\ldots,M, \quad j = 1,2. \tag{22}$$

Details of the estimation of the expansion error are available in [11].

In the case $l = 0$, we rewrite (21) by making use of the Riemann zeta function as follows:

$$B_0^{(j,M)} = C_0^{(j)} + 4h\sum_{\kappa=1}^{K_j} \frac{(-1)^{\kappa}F_j^{(2\kappa-1)}(0)}{(4\pi hM)^{2\kappa}}\zeta(2\kappa) + \mathrm{O}\left\{\frac{8hF_j^{(2K_j+1)}(0)}{(4\pi hM)^{2K_j+2}}\right\}. \tag{23}$$

Details of the estimation of the expansion error are available in [11] as well. Values of the Riemann zeta function required in (23) can be taken from Table 23.3, p. 811 of [1].

For coefficients $B_l^{(j,M)}$ the error of the asymptotic expansions was estimated in (22) for $l = -M+1, \ldots, -1, 1, \ldots, M$:

$$E_{K_j}^{(j,M)} = \mathrm{O}\left[\frac{6h\Delta t F_j^{(2K_j+1)}(0)}{(2\pi hM)^{2K_j+2}}\right], \quad j = 1,2.$$

It is obviously greater than the error for $l = 0$ given in (23). Figs. 2(a) and (b) show graphs of $E_{K_2}^{(2,M)}$ versus K_2 for typical values of L and Δt. Dependence of $E_{K_2}^{(2,M)}$ on h is much weaker and corresponding graphs are not given.

2.4. Crucial aspects of implementation

The accurate calculation of high derivatives of $F_j(\xi)$ for $\xi = 0$ and of $\cot\alpha - \alpha^{-1}$ in (22) and (23) is crucial in the practical implementation of the algorithm.

Starting from computational formulas for $F_2^{(k)}(0)$, we note that it can be represented as a product of three functions $e_N(\pi^2 Dh^2\xi^2)$, $\mathrm{e}^{-\pi^2 Dh^2\xi^2}$, and $1/\mathscr{G}(\xi)$, where

$$\mathscr{G}(\xi) = 1 - \Delta t\sigma_I\mathscr{F}[\mathscr{L}](\xi) = 1 + \Delta t\sigma_I(4\pi^2\xi^2 - \pi\gamma|\xi|). \tag{24}$$

Thus, the application of the Leibniz rule reduces the problem to the evaluation of derivatives of arbitrary orders of the factors. It is easy to see that

$$\left.\frac{\mathrm{d}^n e_N(\pi^2 Dh^2\xi^2)}{\mathrm{d}\xi^n}\right|_{\xi=0} = \begin{cases} (2\mu)!(\pi^2 Dh^2)^\mu/\mu! & \text{for } n = 2\mu,\ \mu = 0,1,2,\ldots,N, \\ 0 & \text{for all other } n, \end{cases}$$

and

$$\left.\frac{\mathrm{d}^n \mathrm{e}^{-\pi^2 Dh^2\xi^2}}{\mathrm{d}\xi^n}\right|_{\xi=0} = \begin{cases} (2\mu)!(-\pi^2 Dh^2)^\mu/\mu! & \text{for } n = 2\mu,\ \mu = 0,1,2,\ldots, \\ 0 & \text{for all other } n. \end{cases} \tag{25}$$

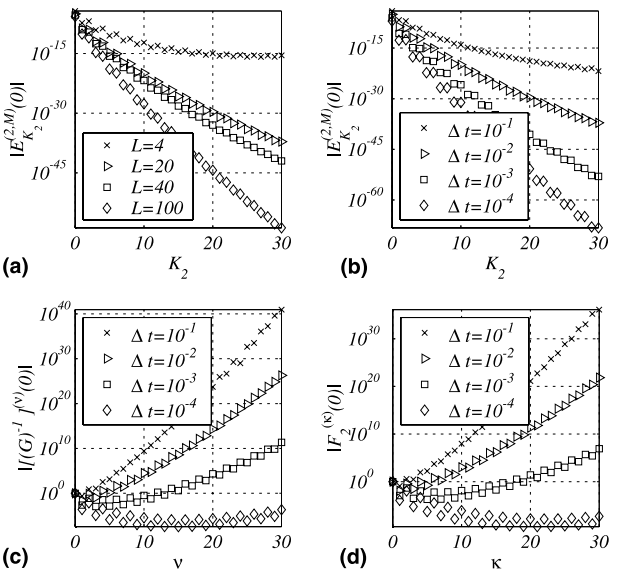

Fig. 2. Dependence of $E_{K_2}^{(2,M)}$ on K_2 for $\Delta t = 0.01$ (a), and $L = 20$ (b). High order derivatives $\{\mathscr{G}^{-1}(\xi)\}^{(\nu)}$ for $\xi = 0$ (c), and values of $|F_2^{(\kappa)}(0)|$ (d). Here $h = 0.01$, $D = 4$, $N = 0$, and $\gamma = 0.8$.

Values of $\{[\mathscr{G}(\xi)]^{-1}\}^{(\nu)}$ for $\xi = 0$ can be obtained with the help of the expansion $(1-x)^{-1} = 1 + x + x^2 + \cdots$ Using it for $[\mathscr{G}(\xi)]^{-1}$ in an ε-vicinity of $\xi = 0$ and, further, differentiating the expansion term-by-term, yields

$$\left.\frac{\mathrm{d}^{\nu}[\mathscr{G}(\xi)]^{-1}}{\mathrm{d}\xi^{\nu}}\right|_{\xi=0} = \nu!\pi^{\nu} \sum_{\mu=\mathrm{ceil}(\nu/2)}^{\nu} \binom{\mu}{2\mu-\nu} (-4)^{\nu-\mu}\gamma^{2\mu-\nu}(\Delta t\sigma_I)^{\mu}.$$

High order derivatives of $\mathscr{G}^{-1}(\xi)$ for $\xi = 0$ may become very large as their order grows, see Fig. 2(c). Fortunately, large values of $\{\mathscr{G}^{-1}(\xi)\}^{(\nu)}$ for $\xi = 0$ are compensated by other factors, and the terms of expansion (22) are eventually decaying as it can be seen from Figs. 2(a) and (b).

Fig. 2(d) shows the graph of $|F_2^{(\kappa)}(0)|$ versus κ for a set of Δt. The saw-shape of the graph is explained by the alternation of the odd-even order of the derivatives. The graph itself is point-wise and is defined for integer values of κ only. Similar to high order derivatives of $\mathscr{G}^{-1}(\xi)$, these functions can become very large for large κ as well and certain care is required in practical implementations of (22) in order to avoid severe round-off errors. In our calculations κ did not exceed 12 usually.

Another important parameter is γ. For $\gamma = 0$ all odd derivatives of $F_2^{(\kappa)}(0)$ vanish, making asymptotic expansions of the previous section senseless and indicating that the convolution coefficients $C_l^{(j)}$ decay exponentially for $l \to \infty$. This is because (2) turns into Burgers' equation for $\gamma = 0$ and is no longer nonlocal. The effect of γ within the range $0.1 \leqslant \gamma \leqslant 1$ and of other parameters on $F_2^{(\kappa)}(0)$ is less pronounced and the corresponding graphs are not shown for the sake of brevity.

The values of $F_1^{(\kappa)}(0)$ can be conveniently expressed in terms of $F_2^{(\kappa)}(0)$:

$$F_1^{(\kappa)}(0) = \begin{cases} \pi\gamma F_2(0), & \kappa = 1, \\ \kappa\pi\gamma F_2^{(\kappa-1)}(0) - 4\kappa(\kappa-1)\pi^2 F_2^{(\kappa-2)}(0), & \kappa = 2, 3, \ldots \end{cases}$$

In order to calculate high order derivatives of $\cot\alpha - \alpha^{-1}$, its power series expansion (see entry 4.3.70, p. 75 of [1]) is employed resulting for $\kappa = 0, 1, 2, \ldots$ in

$$\frac{\mathrm{d}^{2\kappa+1}}{\mathrm{d}\alpha^{2\kappa+1}}(\cot\alpha - \alpha^{-1}) = -\frac{2}{\pi^{2\kappa+2}}\sum_{\mu=1}^{\infty}\zeta(2\mu+2\kappa)\frac{(2\mu+2\kappa-1)!}{(2\mu-2)!}\left(\frac{\alpha}{\pi}\right)^{2\mu-2}. \tag{26}$$

We remind that $\alpha = \pi|l|/2M \leqslant \pi/2$, $l = 1, \ldots, M$ and only derivatives of odd order are used in formulas for convolution coefficients. Unlike the inner series in (21) the series in (26) require a very limited number of summands to be calculated accurately even in the worst case of $\alpha = \pi/2$. It should be taken into account in implementations that for sufficiently large κ and α, the summands of (26) reach their maximum for $\mu \approx (\kappa + 1/2)(\pi/\alpha - 1)^{-1} + 1$.

Besides the infinite summation, formulas (22) and (23) for calculation of $B_l^{(j,M)}$ include values of $C_l^{(j)}$ for $l = -M+1, \ldots, M$. Because of the fast decay of the integrands in (15), numerical integration is very efficient and can be done by standard routines. Unfortunately, the accuracy of these universal algorithms is at most about 3–4 decimal digits less than machine precision. Therefore, in order to reach the accuracy on the level of machine precision, a special tackling of (15) is required. In particular, the function $[\mathscr{G}(\xi)]^{-1}$ from (24) can be approximated by (5), (6) and substituted into (15). The result can be integrated analytically by using [21], p. 452, entry 2.5.36.9. For small enough Δt, when high derivatives of $[\mathscr{G}(\xi)]^{-1}$ are not very large (see Fig. 2(c)), the approximation accuracy of the integrals in (15) can be improved up to the machine zero [16].

3. Computational algorithm in two dimensions

3.1. Discretization

By analogy with the one-dimensional case, we split the computations into two stages

$$(I - \Delta t\sigma_I \mathscr{L})Y^{(n)} = \mathscr{L}\boldsymbol{\Phi}^{(n)} + G^{(n)}, \tag{27}$$

and

$$\left[I - \Delta t\sigma_1 \frac{\partial\boldsymbol{\Phi}^{(n)}}{\partial x_1}\frac{\partial}{\partial x_1}\right]\left[I - \Delta t\sigma_1 \frac{\partial\boldsymbol{\Phi}^{(n)}}{\partial x_2}\frac{\partial}{\partial x_2}\right]\frac{\boldsymbol{\Phi}^{(n+1)} - \boldsymbol{\Phi}^{(n)}}{\Delta t} = Y^{(n)}, \tag{28}$$

where, on this occasion,

$$\mathscr{L}\boldsymbol{\Phi} = \frac{\partial^2\boldsymbol{\Phi}}{\partial x_1^2} + \frac{\partial^2\boldsymbol{\Phi}}{\partial x_2^2} - \frac{\gamma}{4\pi}\Delta\int_{\mathbb{R}^2}\frac{\boldsymbol{\Phi}(y_1, y_2, t)\,\mathrm{d}\boldsymbol{y}}{|\boldsymbol{x} - \boldsymbol{y}|},$$

$$G^{(n)} = \frac{\sigma_1 + \sigma_2}{2}\left[\left(\frac{\partial\boldsymbol{\Phi}^{(n)}}{\partial x_1}\right)^2 + \left(\frac{\partial\boldsymbol{\Phi}^{(n)}}{\partial x_2}\right)^2\right] + \frac{1 - \sigma_1 - \sigma_2}{2}\left[\left(\frac{\partial\boldsymbol{\Phi}^{(n-1)}}{\partial x_1}\right)^2 + \left(\frac{\partial\boldsymbol{\Phi}^{(n-1)}}{\partial x_2}\right)^2\right],$$

$$\boldsymbol{x} = (x_1, x_2), \quad \boldsymbol{y} = (y_1, y_2), \quad \text{and} \quad \boldsymbol{\Phi}^{(n)} = \boldsymbol{\Phi}(x_1, x_2, n\Delta t), \quad n = 0, 1, \ldots$$

Again, after a finite difference approximation of space derivatives, the solution to (28) can be obtained by forward and backward sweeps of LU decomposition. The solution to (27) in terms of the Fourier transform is

$$Y^{(n)}(\boldsymbol{x}) = \int_{\mathbb{R}^2}\frac{\mathscr{F}[\mathscr{L}](\boldsymbol{\xi})\mathscr{F}[\boldsymbol{\Phi}^{(n)}](\boldsymbol{\xi}) + \mathscr{F}[G^{(n)}](\boldsymbol{\xi})}{1 - \Delta t\sigma_I\mathscr{F}[\mathscr{L}](\boldsymbol{\xi})}\mathrm{e}^{\mathrm{i}2\pi(\boldsymbol{\xi}\cdot\boldsymbol{x})}\,\mathrm{d}\boldsymbol{\xi}, \tag{29}$$

where $\mathscr{F}[\mathscr{L}](\xi) = -4\pi^2|\boldsymbol{\xi}|^2 + \pi\gamma|\boldsymbol{\xi}|$, and $\boldsymbol{\xi} = (\xi_1, \xi_2)$.

The approximation formula (5) in two dimensions takes the form

$$g(\boldsymbol{x}) \approx g_h(\boldsymbol{x}) = \frac{1}{D} \sum_{\boldsymbol{m}\in\mathbb{Z}^2} g_{\boldsymbol{m}} \eta_{\mathcal{N}}\left(\frac{\boldsymbol{x}-\boldsymbol{m}h}{\sqrt{D}h}\right), \tag{30}$$

where $\boldsymbol{m} = (m_1, m_2)$ and $g_{\boldsymbol{m}} = g(\boldsymbol{m}h)$. As basis function one can use

$$\eta_{\mathcal{N}}(\boldsymbol{x}) = \eta_{2N+2}(\boldsymbol{x}) = \frac{1}{\pi} e_N\left(-\frac{1}{4}\Delta\right) \mathrm{e}^{-|\boldsymbol{x}|^2} = \frac{\mathrm{e}^{-|\boldsymbol{x}|^2}}{\pi} \mathrm{L}^{(1)}_{N+1}(|\boldsymbol{x}|^2), \tag{31}$$

where

$$L^{(1)}_{N+1}(y) = \frac{\mathrm{e}^y y^{-1}}{(N+1)!}\left(\frac{\mathrm{d}}{\mathrm{d}y}\right)^{N+1} (\mathrm{e}^{-y} y^N)$$

is the generalized Laguerre polynomial of order $N+1$. Similar to the one-dimensional case, formula (30) with (31) provides approximation of order $\mathrm{O}(h^{2N+2})$ plus a small saturation term of order $\mathrm{O}(\mathrm{e}^{-\pi^2 D})$, see [15,16].

The Fourier transform of (30) is

$$\mathscr{F}[g](\boldsymbol{\xi}) \approx \mathscr{F}[g_h](\boldsymbol{\xi}) = h^2 e_N(\pi^2 D h^2 |\boldsymbol{\xi}|^2) \mathrm{e}^{-\pi^2 D h^2 |\xi|^2} \sum_{\boldsymbol{m}\in\mathbb{Z}^2} g_{\boldsymbol{m}} \mathrm{e}^{-2\pi \mathrm{i} h(\boldsymbol{m}\cdot\boldsymbol{\xi})}. \tag{32}$$

Substitution of (32) into (29) results in the convolution

$$Y^{(n)}_{\boldsymbol{k}} = \sum_{\boldsymbol{m}\in\mathbb{Z}^2} C^{(1)}_{\boldsymbol{k}-\boldsymbol{m}} \Phi^{(n)}_{\boldsymbol{m}} + C^{(2)}_{\boldsymbol{k}-\boldsymbol{m}} G^{(n)}_{\boldsymbol{m}}, \quad \boldsymbol{k} \in \mathbb{Z}^2, \tag{33}$$

with coefficients

$$C^{(j)}_{\boldsymbol{l}} = 2\pi h^2 \int_0^\infty \xi F_j(\xi) J_0(2\pi h |\boldsymbol{l}| \xi) d\xi, \quad j = 1, 2, \ \ \boldsymbol{l} \in \mathbb{Z}^2, \tag{34}$$

where $J_0(x)$ is the Bessel function of zero order and $F_j(\xi)$ are exactly the same as in the one-dimensional case, i.e., are given by formulas (16). These coefficients are even functions of both components of index $\boldsymbol{l}$, and $C^{(1)}_{\boldsymbol{l}} = (\sigma_I \Delta t)^{-1}[C^{(2)}_{\boldsymbol{l}} - \eta_{\mathcal{N}}(h\boldsymbol{l})]$ for $\boldsymbol{l} \in \mathbb{Z}^2$.

Considering space periodic solutions and assuming that their period $\boldsymbol{L} = (L, L)$ is commensurable with the discretization parameter h, i.e., $L/h = 2M \in \mathbb{Z}$, we have: $\Phi^{(n)}_{\boldsymbol{m}} = \Phi^{(n)}_{\boldsymbol{m}+2\boldsymbol{M}}$, $G^{(n)}_{\boldsymbol{m}} = G^{(n)}_{\boldsymbol{m}+2\boldsymbol{M}}$, $\boldsymbol{m} \in \mathbb{Z}^2$, where $\boldsymbol{M} = (M, M)$. Then, formula (33) can be transformed into

$$Y_{\boldsymbol{k}} = \sum_{m_1=k_1-M}^{k_1+M-1} \sum_{m_2=k_2-M}^{k_2+M-1} B^{(1,M)}_{\boldsymbol{k}-\boldsymbol{m}} \Phi^{(n)}_{\boldsymbol{m}} + B^{(2,M)}_{\boldsymbol{k}-\boldsymbol{m}} G^{(n)}_{\boldsymbol{m}}, \tag{35}$$

where $-M \leqslant k_1, k_2 \leqslant M-1$ and

$$B^{(j,M)}_{\boldsymbol{l}} = \sum_{\boldsymbol{\mu}\in\mathbb{Z}^2} C^{(j)}_{\boldsymbol{l}-2M\boldsymbol{\mu}} = C^{(j)}_{\boldsymbol{l}} + \sum_{\boldsymbol{\mu}\in\mathbb{Z}^2\setminus\{\boldsymbol{0}\}} C^{(j)}_{\boldsymbol{l}-2M\boldsymbol{\mu}}, \tag{36}$$

for $-M+1 \leqslant l_1, l_2 \leqslant M$ and $j = 1, 2$. The functions $\Phi^{(n)}_{\boldsymbol{m}}$ and $G^{(n)}_{\boldsymbol{m}}$ are involved in (35) for $-2M \leqslant m_1, m_2 \leqslant 2M-2$.

Similarly to the one-dimensional case, the sum (35) can be transformed into the discrete circular convolution and calculated by using two-dimensional FFT, see [28].

3.2. Convolution coefficients

In two dimensions the convolution coefficients (34) have a form of the Hankel transform of the zero order and for large enough values of $|\boldsymbol{l}|$, their integrands will frequently oscillate as well. However, the application of the Laplace method of asymptotic approximation of the integral is not straightforward because of the lack of a theorem similar to Lebesgue's one for Fourier integrals.

In order to obtain an asymptotic expansion of (34) for $|\boldsymbol{l}| \to \infty$ we consider the integral

$$\int_0^\infty Q(\xi)\mathrm{e}^{-a\xi^2} J_0(b\xi)\,\mathrm{d}\xi \tag{37}$$

for a sufficiently smooth function $Q(\xi)$ and large $b > 0$. By virtue of the rapid decay of the integrand, we assume that the nonnegligible contribution to the integral comes from a vicinity of $\xi = 0$, where $Q(\xi)$ can be represented by the Taylor series. Then, integral (37) can be approximated by a linear combination of integrals with $Q(\xi) = \xi^n$, $n = 0, 1, 2, \ldots$ The latter can be written in terms of the confluent hypergeometric function (see entry 2.12.9.3, p. 186 of [21]). The asymptotic of this function for $b \to \infty$ and even n is given in entry 13.5.1, p. 508 of [1]. For odd values of n the asymptotic is exponential and the contribution from corresponding terms into (37) is asymptotically negligible.

Carrying out all these substitutions and appropriate regrouping of summands yields

$$\begin{aligned}\int_0^\infty Q(\xi)\mathrm{e}^{-a\xi^2} J_0(b\xi)\,\mathrm{d}\xi = {} & \sum_{\kappa=0}^{K} \frac{(-1)^\kappa(2\kappa)!}{(2^\kappa\kappa!)^2 b^{2\kappa+1}} \left.\frac{\mathrm{d}^{2\kappa} Q(\xi)\mathrm{e}^{-a\xi^2}}{\mathrm{d}\xi^{2\kappa}}\right|_{\xi=0} \\ & + \mathrm{O}\left\{ \frac{(2K+2)!}{[2^{K+1}(K+1)!]^2 b^{2K+3}} \left.\frac{\mathrm{d}^{2K+2} Q(\xi)\mathrm{e}^{-a\xi^2}}{\mathrm{d}\xi^{2K+2}}\right|_{\xi=0} \right\}\end{aligned} \tag{38}$$

for $b \to \infty$. Here we also used (25) for high order derivatives of $\mathrm{e}^{-a\xi^2}$, the Leibniz' formula for differentiation of a product of functions and the expression of the gamma function of a half-integer argument in terms of factorial $\Gamma(m + 1/2) = \sqrt{\pi}2^{-2m}(2m)!/(m)!$ Turning back to (34), we have

$$\begin{aligned} C_{\boldsymbol{l}}^{(j)} = {} & 2\pi h^2 \sum_{\kappa=0}^{K} \frac{(-1)^\kappa(2\kappa)!}{(2^\kappa\kappa!)^2 (2\pi h|\boldsymbol{l}|)^{2\kappa+1}} \left.\frac{\mathrm{d}^{2\kappa}\xi F_j(\xi)}{\mathrm{d}\xi^{2\kappa}}\right|_{\xi=0} + \mathrm{O}\left\{ \frac{2\pi h^2 (2K+2)!}{[2^{K+1}(K+1)!]^2 (2\pi h|\boldsymbol{l}|)^{2K+3}} \left.\frac{d^{2K+2}\xi F_j(\xi)}{d\xi^{2K+2}}\right|_{\xi=0} \right\}, \\ & j = 1, 2. \end{aligned} \tag{39}$$

One can see that $C_{\boldsymbol{l}}^{(j)} \sim |\boldsymbol{l}|^{-3}$ for $|\boldsymbol{l}| \to \infty$ because of $\xi F(\xi)|_{\xi=0} = 0$.

From (36), (39) and because of the relationship $d^{2\kappa}\xi F_j(\xi)/d\xi^{2\kappa}|_{\xi=0} = 2\kappa F_j^{(2\kappa-1)}(0)$, we have

$$B_{\boldsymbol{l}}^{(j,M)} = C_{\boldsymbol{l}}^{(j)} + 2\pi h^2 \sum_{\kappa=1}^{K} \frac{(-1)^\kappa 2\kappa(2\kappa)!\Psi_\kappa(\boldsymbol{l}/2M)}{(2^\kappa\kappa!)^2 (4\pi hM)^{2\kappa+1}} F_j^{(2\kappa-1)}(0) + \mathrm{O}\left\{ \frac{4h^2\sqrt{\pi(K+1)}\Psi_{K+1}(\boldsymbol{l}/2M)}{(4\pi hM)^{2K+3}} F_j^{(2K+1)}(0) \right\}, \tag{40}$$

where $-M + 1 \leqslant l_1, l_2 \leqslant M$, $j = 1, 2$,

$$\Psi_v(\boldsymbol{\alpha}) = \sum_{\boldsymbol{\mu}\in\mathbb{Z}^2\setminus\{\mathbf{0}\}} \frac{1}{|\boldsymbol{\alpha}-\boldsymbol{\mu}|^{2v+1}}, \tag{41}$$

and the upper bound was used in the error term of the expansion.

3.3. Crucial implementation issues and parallelization

The calculation of high order derivatives of $F_j(\xi)$ for $\xi = 0$ has been considered in Section 2.4. So, the only remaining problem in computing the coefficients $B_{\boldsymbol{l}}^{(j,M)}$ is the estimation of the series (41). Cutting this series off at $|\boldsymbol{\mu}| = M_\infty$, results in the residual of order M_∞^{-2v+1}, which, similar to the one-dimensional case, gives in the worst case $v = 1$ the rate of convergence M_∞^{-1}. Taking into account the two-dimensional nature of (41), this makes it even less realistic to calculate the sum directly.

In order to accelerate the convergence of series (41), we apply a kind of Kummer's transformation as follows:

$$\begin{aligned}\Psi_v(\boldsymbol{\alpha}) = \sum_{\boldsymbol{\mu}\in\mathbb{Z}^2\setminus\{0\}} \Bigg(& |\boldsymbol{\alpha}-\boldsymbol{\mu}|^{-2v-1} - \sum_{\lambda_1=0}^{\Lambda_v}\sum_{\lambda_2=0}^{\Lambda_v} \frac{\alpha_1^{\lambda_1}\alpha_2^{\lambda_2}}{\lambda_1!\lambda_2!} \left.\frac{\partial^{\lambda_1+\lambda_2}|\boldsymbol{\alpha}-\boldsymbol{\mu}|^{-2v-1}}{\partial\alpha_1^{\lambda_1}\partial\alpha_2^{\lambda_2}}\right|_{\boldsymbol{\alpha}=0}\Bigg) \\ & + \sum_{\lambda_1=0}^{\Lambda_v}\sum_{\lambda_2=0}^{\Lambda_v} \frac{\alpha_1^{\lambda_1}\alpha_2^{\lambda_2}}{\lambda_1!\lambda_2!} \sum_{\boldsymbol{\mu}\in\mathbb{Z}^2\setminus\{0\}} \left.\frac{\partial^{\lambda_1+\lambda_2}|\boldsymbol{\alpha}-\boldsymbol{\mu}|^{-2v-1}}{\partial\alpha_1^{\lambda_1}\partial\alpha_2^{\lambda_2}}\right|_{\boldsymbol{\alpha}=0}.\end{aligned} \tag{42}$$

The residual of the transformed series cut off at $|\boldsymbol{\mu}| = M_\infty$ is of order $M_\infty^{-2v-1+\Lambda_v}$, and by choosing a proper value of Λ_v it is easy to obtain the required accuracy of summation for practically acceptable values of M_∞ of order 100.

Transformation (42) reduces the problem of summation of (41) to the calculation of numbers

$$\sum_{\boldsymbol{\mu}\in\mathbb{Z}^2\setminus\{0\}} \left.\frac{\partial^{\lambda_1+\lambda_2}|\boldsymbol{\alpha}-\boldsymbol{\mu}|^{-2v-1}}{\partial\alpha_1^{\lambda_1}\partial\alpha_2^{\lambda_2}}\right|_{\boldsymbol{\alpha}=0} \tag{43}$$

for a set of integer parameters λ_1, λ_2, and v. For $v > 4$ the series (41) converge reasonably fast without any transformations. For $v \leqslant 4$, in order to provide accuracy of summation on the level of machine precision, it is sufficient to take $\Lambda_v = 6 - 2(v-1)$.

All practically important cases of (43) can be reduced to the values of the series

$$\psi_{\lambda,v}^{(j)} = \sum_{\boldsymbol{\mu}\in\mathbb{Z}^2\setminus\{0\}} \frac{\mu_j^{2\lambda}}{(\mu_1^2+\mu_2^2)^{v+1/2}}, \quad j = 1,2, \tag{44}$$

for $1 \leqslant v \leqslant 7$ and $\max\{v-4,0\} \leqslant \lambda \leqslant \mathrm{int}[(v-1)/2]$. Generally speaking, we would have to consider infinite sums of terms like $\mu_1^{\tilde{\lambda}_1}\mu_2^{\tilde{\lambda}_2}|\boldsymbol{\mu}|^{-2v-1}$. However, if at least one of $\tilde{\lambda}_j$, $j = 1,2$, is odd, then the contribution of the corresponding series to (43) will be zero. On the other hand, terms with both even $\tilde{\lambda}_j$ can be reduced to a linear combination of (44). For example, $\mu_1^2\mu_2^2|\boldsymbol{\mu}|^{-2v-1} = (\mu_1^2\mu_2^2 + \mu_2^4 - \mu_2^4)|\boldsymbol{\mu}|^{-2v-1} = \mu_2^2|\boldsymbol{\mu}|^{-2v+1} - \mu_2^4|\boldsymbol{\mu}|^{-2v-1}$. Obviously, $\psi_{\lambda,v}^{(1)} = \psi_{\lambda,v}^{(2)}$, which gives immediately

$$\psi_{1,v}^{(j)} = \frac{1}{2}\psi_{0,v-1}^{(j)} = \frac{1}{2}\sum_{\boldsymbol{\mu}\in\mathbb{Z}^2\setminus\{0\}} \frac{1}{(\mu_1^2+\mu_2^2)^{v-1/2}}, \quad j = 1,2. \tag{45}$$

Unfortunately, the symmetry in j does not help so much for $\lambda > 1$.

For $\lambda \geqslant 0$ series (44) can be rewritten as follows:

$$\psi_{\lambda,v}^{(j)} = 2[1+\mathrm{sign}(\lambda)]\zeta(2v-2\lambda+1) + 4\sum_{\mu_1=1}^{\infty}\sum_{\mu_2=1}^{\infty}\frac{\mu_j^{2\lambda}}{(\mu_1^2+\mu_2^2)^{v+1/2}},$$

where the series in the right-hand side can be represented by the formula

$$\begin{aligned}\sum_{\mu_1=1}^{\infty}\sum_{\mu_2=1}^{\infty}\frac{\mu_j^{2\lambda}}{(\mu_1^2+\mu_2^2)^{v+1/2}} = \frac{2^{-2v+2\lambda}\sqrt{\pi}}{\Gamma(v+1/2)}\sum_{\kappa_1=0}^{\lambda}c_{\lambda,\kappa_1}(v)\Bigg[&\frac{\sqrt{\pi}\Gamma(2v-2\lambda)\zeta(2v-2\lambda)}{2^{\kappa_1}\Gamma(v-2\lambda+\kappa_1+1/2)}\\ &-\frac{\Gamma(2v-2\lambda+1)\zeta(2v-2\lambda+1)}{2^{\kappa_1+1}\Gamma(v-2\lambda+\kappa_1+1)}\\ &+\frac{(-1)^{\lambda-\kappa_1}}{2^{\lambda-1}}\sum_{\kappa_2=1}^{\infty}\sum_{\kappa_3=1}^{\infty}\left(\frac{4\pi\kappa_2}{\kappa_3}\right)^{v-\lambda}\mathscr{D}_{v-\lambda}^{(2\lambda-2\kappa_1)}(2\pi\kappa_2\kappa_3)\Bigg].\end{aligned} \tag{46}$$

Expressions for $\mathscr{D}_{v-\lambda}^{(2\lambda-2\kappa_1)}$ and numerical values of a few series (44) relevant to this paper are given in Appendix A. Details of the evaluation of this formula are available in [11].

In contrast to the terms of the double series in the left-hand side of (46), terms of the double series in the right decay exponentially and, within the required values of integer parameters v and λ, accuracy on the level of machine zero $\varepsilon_M \approx 10^{-16}$ is reached for $\kappa_2,\ \kappa_3 \leqslant 10$. In practice, a generic work station had calculated all the required numbers (46) in a fraction of a second. The calculations were carried out in Matlab and results are given in Appendix A too. The algorithm was validated by comparison with the direct summation for large enough values of v and with formula (45).

The coefficients $C_{\boldsymbol{l}}^{(j)}$ from (40) were calculated by direct numerical integration. Similarly to the one-dimensional case, the integrands in (34) are very smooth and fast decaying functions which makes integration very efficient. The only difference is that the integration should be done on the sequence of intervals between zeros of $J_0(2\pi h|\boldsymbol{l}|\xi)$, see, e.g. [1], rather than between zeros of $\cos(2\pi h l\xi)$. An attempt to accelerate the convergence by the ε-algorithm halved processing time, on average, but failed to produce reliable estimation of the accuracy. Thus, if accuracy is of primary interest, then it is safer to carry out the integration straightforwardly.

The convolution coefficients (40) are point-wise and the parallelization of their calculations represents no problems. On average, in our practice, these calculations take about the same amount of computer resources as a few dozens of time steps. In contrast, at least a few dozens of thousands of time steps is usually required in order to obtain the numerical solution to (1) on a physically meaningful time scale.

In parallel implementation, the coordinate direction-wise nature of the time marching algorithm suggests to split the core data of $4M \times 4M$ elements between P processors in the form of P arrays of $4M \times (4M/P)$ elements. The repeating alteration of processing between x_1 and x_2 directions prompts to keep a copy of the data split between processors along another direction into P arrays of $(4M/P) \times 4M$ elements as well (see Fig. 3). Optimal load balancing is reached by setting P as a factor of $4M$.

Computational codes were written in Fortran 90 and in the two dimensional case MPI has been chosen as the parallelization tool. The chosen data structure allows efficient use of the standard sequential routines for the discrete Fourier transform in (35) and LU-sweeps in (28).

The MPI code was validated by comparison against the results obtained with the sequential code for a relatively small computational domain with $L = 10\pi$. The discrepancy was on a level of 3–4 decimal digits less than machine precision, which is in a good agreement with the accuracy of the quadrature routines used by the parallel code. The sequential code was run on Origin 200 and the parallel one on CRAY T3E-1200. For 128 processors and main data arrays of 512×512 elements the efficient level of parallelization was about 23%. It looks like that the main contribution into the degradation of the efficiency of parallelization

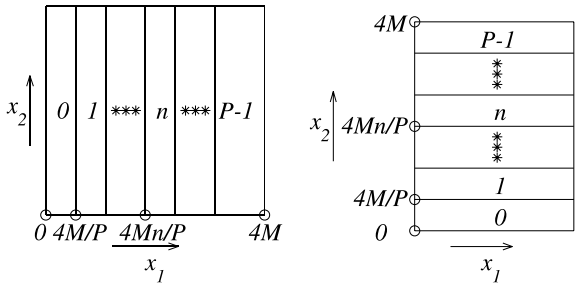

Fig. 3. Two copies of data distributed among P processors in x_2 and x_1 directions.

comes from the MPI_GATHERV procedure which is used repeatedly during every time step in order to transform data arrays from x_1 to x_2 orientation and vice verse (see Fig. 3).

4. Results of numerical experiments

4.1. Accuracy

The accuracy of the algorithm was tested on steady coalescent pole solutions (4) in relatively small domains $L < L_c$. For $N_p = 1$, the steady-state solution corresponds to $b_1 = (L/4\pi)\ln[(\gamma L + 4\pi)/(\gamma L - 4\pi)]$. For $N_p > 1$ the values of $b_1, \ldots, b_{N_p}$ were calculated by Newton iterations as steady-state solutions to the pole dynamics system.

In practice, for numerical grids with $0.001 < h < 0.1$, the theoretical order of approximation was reached for up to the fourth order of approximation. For algorithms of higher orders real approximation was not better than of the fifth order. Therefore, from the point of view of computational efficiency, it is expedient to use the algorithm of at most of the sixth order or even of the fourth one for this range of h. In our practice, by proper choice of D, h, and of the order of approximation, it was always possible to obtain the relative residual of the approximation of (2) on the steady coalescent pole solutions up to 10^{-10}.

Limitations of the accuracy of the algorithm come from variety of reasons. In particular, from errors of the numerical integration to compute the convolution coefficients (15) in (22). Further, high order derivatives of steady coalescent N_p-pole solutions grow very fast with their order. Hence, the high formal order of the approximation might only be observed for smaller values of h than those used in this work.

It was possible to reach the relative accuracy of approximation of the stabilized solution to (2) in comparison to $\Phi_{N_{p,L}}(x,t)$ of order 10^{-10} for $\gamma L < 12\pi$ (i.e., for $N_{p,L} = 1$) as well. However, this accuracy of the approximation of $\Phi_{N_{p,L}}(x,t)$ by the steady state of (2) was rapidly degrading with L growing. This degradation of the accuracy of the stabilized numerical solution is in agreement with the high sensitivity of the steady coalescent pole solutions to noise. Taking into account results of [8], some of the constants C_i, $i = 1,2,3$ in the a priori estimation

$$\|\Phi_{N_{p,L}}(x,t) - \lim_{t\to\infty}\Phi_h(x,t)\|_2 \leqslant C_1 h^N + C_2\varepsilon(D) + C_3\varepsilon_M \tag{47}$$

might be of order of $e^{O(L)}$. Assuming that the round-off errors are pseudorandom, it is most likely that C_3 is of order of $e^{O(L)}$. However, other constants can be much less because the transient amplification usually occurs for perturbations of very special type only, to which the deterministic approximation residuals may not to belong if $\Phi \approx \Phi_{N_{p,L}}$.

The last issue relevant to the accuracy, which we would like to mention here, is the Φ- and x-shift invariance of the Sivashinsky equation. In other words, it means that if $\Phi(x,t)$ is a solution, then, for any real $\Delta\Phi$ and Δx, the function $\Phi(x+\Delta x,t)+\Delta\Phi$ satisfies the Sivashinsky equation as well. Thus, the shifts of the stabilized solution are not known a priori and should be identified in order to allow comparison with the exact solution. The only way to estimate the shifts is by a kind of optimization. In particular, calculation of the minimum of the stabilized solution was carried out in this work. Generally speaking, errors of the estimation of the minimum might interfere or even supersede the errors made during the calculation of the solution itself.

It can be checked by direct substitution that if $\Phi^{(1)}(x,t)$ and $\Phi^{(2)}(x,t)$ are solutions to one-dimensional equation (2), then the function

$$\Phi(x_1,x_2,t)=\Phi^{(1)}(x_1,t)+\Phi^{(2)}(x_2,t) \tag{48}$$

is a solution to the two dimensional equation (1). In our numerical experiments the functions

$$\Phi_{N_{\mathrm{p},L}}(x_1,x_2,t)=\Phi_{N_{\mathrm{p},L}}(x_1,t)+\Phi_{N_{\mathrm{p},L}}(x_2,t) \tag{49}$$

were found to be the steady attractors for Sivashinsky's equation in two dimensions for small enough L. These solutions were used in order to test the accuracy of the algorithm in two space dimensions.

The parameters of the two-dimensional algorithm have a similar qualitative effect on its accuracy as in the one-dimensional case. However, quantitatively, the accuracy of the algorithm in two-dimensions is usually less by one or two decimal digits for the same sets of parameters. Also, understandably, the choice of two-dimensional grids with small values of h is more restrictive in practice.

4.2. One-dimensional equation

The typical evolution of the flame front in a relatively small domain $L=50\pi<L_{\mathrm{c}}$ is shown in Fig. 4. In the very beginning the flame rapidly approaches a steady coalescent N_{p,L_0}-pole solution with the period $L_0=10\pi$ of the initial condition. Later, the solution undergoes a series of bifurcations and stabilizes to the steady coalescent $N_{\mathrm{p},L}$-pole solution with the period L occupying the entire computational domain.

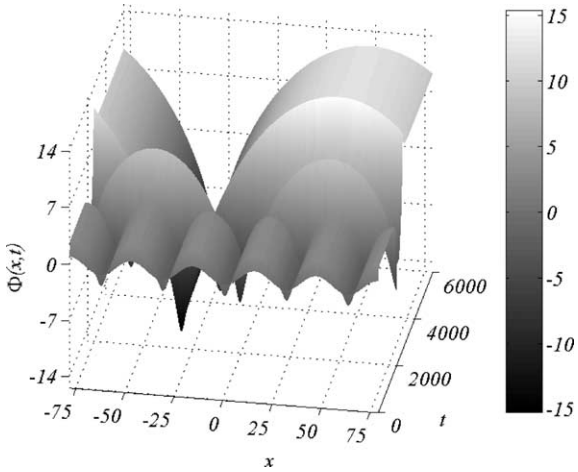

Fig. 4. Evolution of the flame front profile in time for $L=50\pi$, $\gamma=0.8$, and $\Phi(x,0)=-\cos 10\pi x/L$.

Appearance and disappearance of poles in $\Phi(x,t)$ can be clearly seen in the graph of its spatially averaged time derivative:

$$\langle \Phi_t \rangle = L^{-1} \int_{-L/2}^{L/2} \frac{\partial \Phi}{\partial t} \, \mathrm{d}x. \tag{50}$$

Physically, $\langle \Phi_t \rangle$ is the increase of the speed of the flame front in comparison with the speed of the plane laminar flame. For steady coalescent N_p-pole solution (4) we obviously have

$$\langle \Phi_t \rangle = 2\pi N_\mathrm{p} L^{-1} (\gamma - 4\pi N_\mathrm{p} L^{-1}). \tag{51}$$

The behaviour of $\langle \Phi_t \rangle$ for time-dependent solutions to (2) is essentially different. In moments of time which, in terms of (4), correspond to a change in the number of poles per period, function (50) develops sharp spikes, see Fig. 5(a). The Figure shows also that with time all such spikes die out eventually, indicating stabilization of the solution to $\Phi_{N_\mathrm{p},L}(x)$ for any initial conditions. The function $\langle \Phi_t \rangle$ does not develop sharp spikes for time-dependent pole solutions (4) because the number of poles is the integral of the pole dynamics system.

The scenario changes dramatically when the length of the computational domain exceeds a critical value L_c. In this case, sharp spikes in $\langle \Phi_t \rangle$ do not die out but appear and appear for as long as computations are continued, see Fig. 5(b). For some initial conditions transition to the pronounced time-dependent behaviour for $t \to \infty$ can be quite delayed, as it is illustrated in Fig. 5(d) for $L = 100\pi$. Close examination of solutions to (2) shows that the appearance of spikes coincides with the appearance of micro cusps on the surface of the flame front as illustrated in Fig. 1. In terms of pole solutions (4) these micro cusps would correspond to additional poles appearing near the crest of the flame profile, then moving slowly towards its trough, and eventually disappearing there. The change in the temporal behaviour of $\langle \Phi_t \rangle$ for $L < L_\mathrm{c}$ and $L > L_\mathrm{c}$ is further illustrated in Fig. 5(c). Thus, temporal behaviour of numerical solutions to the Sivashinsky equation obtained here with the method of

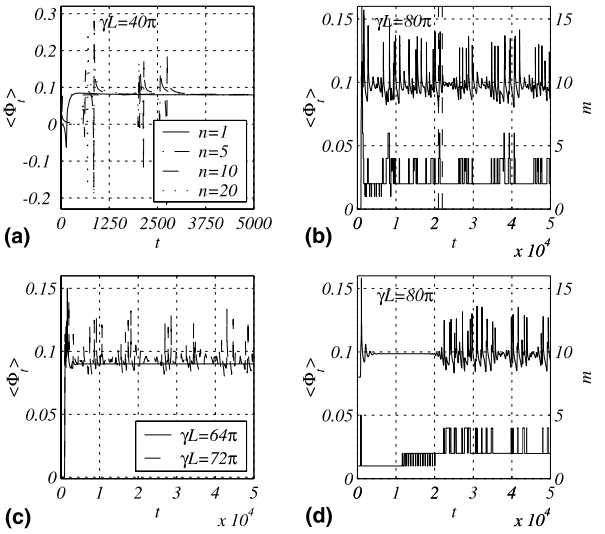

Fig. 5. Dependence of $\langle \Phi_t \rangle$ and the number m of local extremums on the flame surface (lower curve in (b) and (d)) on time. The time interval marked with the dashed lines in (b) corresponds to the appearance of cusps depicted in Fig. 1. Here $\gamma = 0.8$; $\Phi(x,0) = \Phi_{N_\mathrm{p},L}(x,0)$ in (d), and $\Phi(x,0) = -\cos n\pi x/L$ in (a)–(c) with $n = 48$, 52, and 60 for $L = 80\pi$, 90π, and 100π, correspondingly.

saturated asymptotic approximations matches results obtained earlier by the spectral methods, see, e.g. [7,18,22,23].

In order to establish which term in (47) is the dominating one, we ran a series of calculations with varied values of h, D, N and Δt. It was noticed that the effect of these parameters on the accuracy of the stabilized solution disappears when L grows and approaches L_c. Also, the accuracy itself degrades dramatically when L grows and for $L > L_c \approx 85\pi$ numerical solutions do not stabilize at all. On the other hand, the accuracy of the stabilized solution for L close enough to L_c and the value of L_c itself strongly depend on ε_M. This is a clear indication that for large enough L the dominating term in (47) is $C_3\varepsilon_M$. Two values of L_c obtained in our calculations with 32- and 64-bit arithmetic are shown in Fig. 6. The problem of finding the value of L_c by direct numerical simulations is rather time consuming. However, the accuracy of observations was at least $\pm 4\pi$. Note, that corresponding machine zeros were $\varepsilon_M \approx 10^{-7}$ and 10^{-16}.

Strictly speaking, in calculations with spectral methods stabilization of numerical solutions does not happen at all, unless an additional condition of symmetry, e.g., solution is assumed to be an even function, is imposed, see [23]. This gave a reason to the authors of [23] to estimate Lyapunov's exponents for the steady states $\Phi_{N_p,L}(x,t)$, which turned to be very tiny indeed. The dependence of those exponents on machine accuracy was not checked. Though, in view of the recent results in [29] and in this paper, physical meaning of these exponents is not very clear. Stabilization in our computations occurs, probably, because of an implicit positive dissipation intrinsic to the saturated asymptotic approximations, as they are used with large but finite value of the parameter of the order of approximation N.

An analytical attempt to estimate the value of L_c was made in [8] where the following modification of (2) linearized on the steady coalescent pole solution was considered:

$$\frac{\partial \Delta\Phi}{\partial t} - xR^{-1}\frac{\partial \Delta\Phi}{\partial x} = \frac{\partial^2 \Delta\Phi}{\partial x^2} + \frac{\gamma}{2}\frac{\partial \mathscr{H}[\Delta\Phi]}{\partial x}, \quad x \in \mathbb{R}. \tag{52}$$

Here $\Delta\Phi(x,t) = \Phi(x,t) - \Phi_{N_p,L}(x,t)$ and R is the curvature radius in the crest of the flame profile $\Phi_{N_p,L}(x,t)$. The investigation of a particular asymptotic solution to (52) resulted in an estimation of the possible amplification of the spectral density f of harmonics of $\Delta\Phi(x,0)$ versus R. The latter provides values of the critical curvature radius R_c for which the spectral density of the most dangerous harmonics can grow up to the order of $O(1)$. A functional link between L and R can be easily established for $\Phi_{N_p,L}(x,t)$ and the resulting graph of L_c versus f is shown in Fig. 6.

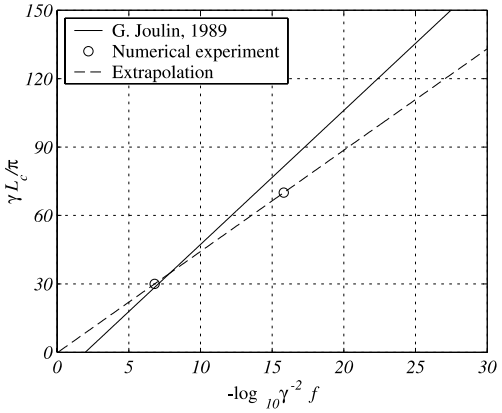

Fig. 6. Dependence of the critical flame size L_c on the strength of the perturbation f.

The agreement is striking because results in [8] were obtained for the spectral density of the most dangerous harmonics of the perturbation $\Delta\Phi(x,0)$ rather than for its amplitude resulting in overestimation of L_c. Also, the value of L_c in [8] corresponds to amplification of the most dangerous harmonic up to the order of O(1), while in our computational practice we were judging L_c by its "stabilized" value of $\langle\Phi_t\rangle$ which results in underestimation of L_c. The use of normalizing parameters κ_1 and κ_2 such that $\kappa_1 f$ and $\kappa_2 O(1)$ replace f and O(1) correspondingly gives exact coincidence of graphs in Fig. 6 for $\kappa_1 \approx 0.81$ and $\kappa_2 \approx 1.32$.

Effect of the round-off errors in numerical solution of (2) can be modelled by a stochastic right-hand side $f(x,t)$ as follows:

$$\frac{\partial\Phi}{\partial t} - \frac{1}{2}\left(\frac{\partial\Phi}{\partial x}\right)^2 = \frac{\partial^2\Phi}{\partial x^2} + \frac{\gamma}{2}\frac{\partial\mathscr{H}[\Phi]}{\partial x} + f(x,t), \quad x \in \mathbb{R}. \tag{53}$$

Such an explicit addition to the Sivashinsky equation was studied, for example, in [3–5,19]. Unlike (2) was obtained under the assumption of small heat expansion $\gamma \ll 1$, it can be considered for any value of $\gamma > 0$ and, then, interpreted for a physically acceptable value of γ' in a larger domain L' in virtue of the invariance condition $\gamma L = \gamma' L'$, see (3). With addition of the noise term in (53) one has to request also, that the noise level in a realistic system with small heat expansion is proportionally smaller $f' = (\gamma')^2\gamma^{-2} f$. This remark is equally true for both explicit and implicit (i.e., round-off errors) noise terms in the Sivashinsky equation.

4.3. Two-dimensional equation

Qualitatively, the temporal behaviour of the two-dimensional flame fronts is similar to the one-dimensional one. Fig. 7 illustrates the evolution of a relatively small flame in two spatial dimensions. Unlike starting from initial condition $\Phi(\boldsymbol{x},0) = -\cos(10\pi x_1/L)\cos(10\pi x_2/L)$, which is not additive in coordinate directions, the solution is rapidly transformed into the additive form (48) and is very close to $\Phi_{1,10\pi}(x_1,t) + \Phi_{1,10\pi}(x_2,t)$ for some time. Later, the first summand begins to evolve and for $t \approx 1050$ the solution is approximately equal to $\Phi_{N_L,L}(x_1,t) + \Phi_{1,10\pi}(x_2,t)$. Only then the second summand begins to bifurcate and the flame front reaches eventually the steady shape composed of the sum of two one-dimensional steady coalescent $N_{p,L}$-pole solutions (49).

Similar scenarios were observed in our simulations with a variety of other initial conditions and values of L. In all the cases the period of the intermediate flame shapes of the additive form (48) was determined by the period of the initial condition if the latter was greater than the neutral wavelength $4\pi/\gamma$ of the dispersion relationship associated with (1). For initial conditions with smaller wavelengths the intermediate shape was just close to zero.

The nonstationary asymptotic character of solutions to the two-dimensional Sivashinsky equation for larger L is illustrated in Fig. 8 in the form of the dependence of the spatially averaged speed of the flame front on time. Here, the perturbations, appearing on the flame surface randomly in time, look like cracks aligned parallel to the x_1-axis and moving along the x_2-coordinate. The $x_1 = const$ cross-sections of the cracks are very similar to the micro cusps observed in one spatial dimension. The cracks lined up parallel to the x_2-axis were not observed in our calculations for L up to 90π. This is, probably, because of the asymmetrical treatment of the spatial coordinate directions implemented in the computational algorithm.

It was found out in our calculations with 64-bit arithmetic, that for the two independent spatial dimensions the value of γL_c is likely to be slightly less than 68π, but does not differ from it significantly. In

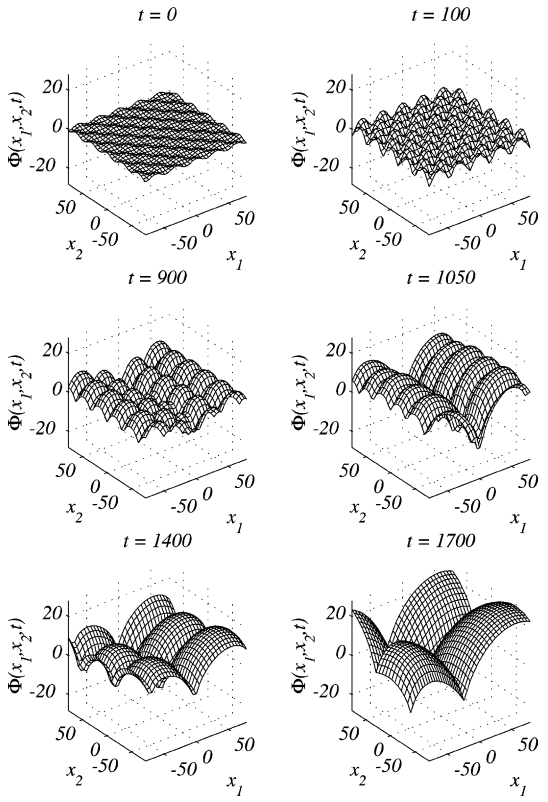

Fig. 7. Evolution of the flame front profile in time for $L = 50\pi$, $\gamma = 0.8$, and $\Phi(x_1, x_2, 0) = -\cos(10\pi x_1/L)\cos(10\pi x_2/L)$.

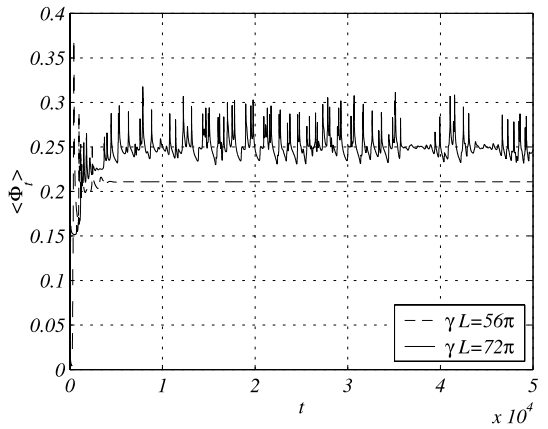

Fig. 8. Dependence of $\langle \Phi_t \rangle$ on time in the two-dimensional case for $L = 70\pi$ and $L = 90\pi$. Here $\gamma = 0.8$ and $\Phi(x_1, x_2, 0) = -\cos(n\pi x_1/L)\cos(n\pi x_2/L)$ with $n = 20$ and 10 for $L = 70\pi$ and 90π, correspondingly.

hydrodynamics, reduction of the critical Reynolds number with the increase of the dimension of the problem is a distinctive characteristic of the nonmodal instability, see [27].

The two-dimensional Sivashinsky equation (1) was not as popular among researchers as its one-dimensional counterpart (2). The paper [18] is one of a few, if not the only one, where (1) was studied nu-

merically. Similar to the one-dimensional case, there is a very good agreement between our results and data from [18], where a spectral method was used.

5. Conclusions

Efficient and high accurate computational algorithms for periodic solutions to the Sivashinsky equation in one and two spatial dimensions were proposed. The algorithms are based on saturated asymptotic approximations. The order of approximation is controlled by an explicit parameter and, generally speaking, the accuracy of the method of saturated asymptotic approximations is only limited by the smoothness of approximated solutions. Results of our calculations are in good quantitative agreement with data obtained by spectral methods.

The implementation of our computational code on CRAY T3E-1200 demonstrated reasonable parallel efficiency of the approach. Resources to improve the performance of the code and the overall efficiency of the computational algorithm were discussed as well. The presented algorithms can be straightforwardly extended to a wide class of nonlinear nonlocal pseudodifferential equations.

For problems in finite computational domains considered in this paper, the method in question has no distinctive advantages in comparison to the spectral methods. There are a few important differences, however. The accuracy of the saturated asymptotic approximations is only degraded locally if the smoothness of the approximated function is lost locally. The latter property of the method proved to be useful for bifurcating solutions with smoothness degrading in moments of bifurcations. Also, the level of implicit numerical dissipation of the proposed algorithm is explicitly controlled by the parameter of the order of approximation. On the other hand, if frequent adjustment of the time step is required, then the proposed approach might be slower than the spectral one because of the necessity to upgrade values of the convolution coefficients. In the finite computational domains the algorithm based on saturated asymptotic approximations is considered as a supplement to the spectral methods. Such a supplement is especially useful when results of numerical simulations are not easy to interpret.

The given examples of computations not only demonstrate the accuracy and efficiency of the algorithms but, also, confirm at a reasonable level of confidence that flame fronts governed by Sivashinsky's equation become extremely sensitive to perturbations as their size grows. This sensitivity was not caused by the special structure of the limiting solutions, formed by a set of coalescent poles, but it is a consequence of the nonnormality of the linearized governing operator. A similar effect was also discovered in many other systems, for example in Hagen–Poiseuille flow, where pole solutions were not found. A possible implication from this sensitivity is that a noise term of physical origins might be required in the Sivashinsky equation in order to retain its physical value for flames of large enough size, see, e.g. [3–5].

Appendix A. Values of the series $\sum_{\boldsymbol{\mu}\in\boldsymbol{Z}^2\setminus\{\mathbf{0}\}}\mu_j^{2\lambda}|\boldsymbol{\mu}|^{-2\nu-1}$

Expressions for $\mathscr{D}^{(2\lambda-2\kappa_1)}_{\nu-\lambda}(2\pi\kappa_2\kappa_3)$ from (46) are given below:

$$\mathscr{D}^{(0)}_{\nu-\lambda}(2\pi\kappa_2\kappa_3) = K_{\nu-\lambda}(2\pi\kappa_2\kappa_3),$$

$$\mathscr{D}^{(2)}_{\nu-\lambda}(2\pi\kappa_2\kappa_3) = K_{\nu-\lambda}(2\pi\kappa_2\kappa_3) - 2\pi\kappa_2\kappa_3 K_{\nu-\lambda+1}(2\pi\kappa_2\kappa_3),$$

$$\mathscr{D}^{(4)}_{\nu-\lambda}(2\pi\kappa_2\kappa_3) = 3K_{\nu-\lambda}(2\pi\kappa_2\kappa_3) - 6(2\pi\kappa_2\kappa_3)K_{\nu-\lambda+1}(2\pi\kappa_2\kappa_3) + (2\pi\kappa_2\kappa_3)^2 K_{\nu-\lambda+2}(2\pi\kappa_2\kappa_3),$$

$$\begin{aligned}\mathscr{D}^{(6)}_{\nu-\lambda}(2\pi\kappa_2\kappa_3) = {} & 15K_{\nu-\lambda}(2\pi\kappa_2\kappa_3) - 45(2\pi\kappa_2\kappa_3)K_{\nu-\lambda+1}(2\pi\kappa_2\kappa_3) \\ & + 15(2\pi\kappa_2\kappa_3)^2 K_{\nu-\lambda+2}(2\pi\kappa_2\kappa_3) - (2\pi\kappa_2\kappa_3)^3 K_{\nu-\lambda+3}(2\pi\kappa_2\kappa_3).\end{aligned}$$

Here $K_n(x)$ are the modified Bessel functions which decay exponentially for $x \to \infty$.

Numerical values of series (44) for parameters relevant to this paper:

$$\sum_{\boldsymbol{\mu}\in\mathbb{Z}^2\setminus\{0\}} |\boldsymbol{\mu}|^{-3} = 9.03362168310095, \qquad \sum_{\boldsymbol{\mu}\in\mathbb{Z}^2\setminus\{0\}} \mu_j^2|\boldsymbol{\mu}|^{-7} = 2.54512911683274,$$

$$\sum_{\boldsymbol{\mu}\in\mathbb{Z}^2\setminus\{0\}} |\boldsymbol{\mu}|^{-5} = 5.09025823366548, \qquad \sum_{\boldsymbol{\mu}\in\mathbb{Z}^2\setminus\{0\}} \mu_j^2|\boldsymbol{\mu}|^{-9} = 2.21155889383922,$$

$$\sum_{\boldsymbol{\mu}\in\mathbb{Z}^2\setminus\{0\}} |\boldsymbol{\mu}|^{-7} = 4.42311778767830, \qquad \sum_{\boldsymbol{\mu}\in\mathbb{Z}^2\setminus\{0\}} \mu_j^2|\boldsymbol{\mu}|^{-11} = 2.09563418137816,$$

$$\sum_{\boldsymbol{\mu}\in\mathbb{Z}^2\setminus\{0\}} |\boldsymbol{\mu}|^{-9} = 4.19126836275633, \qquad \sum_{\boldsymbol{\mu}\in\mathbb{Z}^2\setminus\{0\}} \mu_j^4|\boldsymbol{\mu}|^{-11} = 2.11729427669446,$$

$$\sum_{\boldsymbol{\mu}\in\mathbb{Z}^2\setminus\{0\}} \mu_j^6|\boldsymbol{\mu}|^{-15} = 2.02776956400404, \qquad \sum_{\boldsymbol{\mu}\in\mathbb{Z}^2\setminus\{0\}} \mu_j^4|\boldsymbol{\mu}|^{-13} = 2.05039110312875.$$

References

[1] M. Abramowitz, I.A. Stegun, Handbook of Mathematical Functions, Dover, New York, 1964, republication.

[2] L. Boberg, U. Brosa, Onset of turbulence in a pipe, Zeitschrift für Naturforschung 43a (1988) 697–726.

[3] P. Cambray, G. Joulin, On moderately-forced premixed flames, Twenty–Fourth Symposium (International) on Combustion, The Combustion Institute, 1992, pp. 61–67.

[4] P. Cambray, K. Joulain, G. Joulin, Mean evolution of wrinkle wavelengths in a model of weakly-turbulent premixed flame, Combustion Science and Technology 103 (1994) 265–282.

[5] P. Cambray, G. Joulin, Length-scales of wrinkling of weakly-forced, unstable premixed flames, Combustion Science and Technology 97 (1994) 405–428.

[6] C. Chapman, Onset of turbulence in a pipe, Journal of Fluid Mechanics 120 (2002) 1–50.

[7] S. Gutman, G.I. Sivashinsky, The cellular nature of hydrodynamic flame instability, Physica D 43 (1990) 129–139.

[8] G. Joulin, On the hydrodynamic stability of curved premixed flames, J. Phys. France 50 (1989) 1069–1082.

[9] V. Karlin, V. Maz'ya, Time-marching algorithms for nonlocal evolution equations based upon approximate approximations, SIAM Journal on Scientific Computing 18 (3) (1997) 736–752.

[10] V. Karlin, V. Maz'ya, A.B. Movchan, J.R. Willis, R. Bullough, Numerical solution of nonlinear hypersingular integral equations of the Peierls type in dislocation theory, SIAM Journal on Applied Mathematics 60 (2) (2000) 664–678.

[11] V. Karlin, V. Maz'ya, G. Schmidt, Numerical algorithms to calculate periodic solutions of the Sivashinsky equation, Preprint No. 771, WIAS, Berlin, 2002.

[12] L. Landau, On the theory of slow combustion, Acta Physicochimica URSS XIX (1) (1944) 77–85.

[13] A. Leonard, Computing three-dimensional incompressible flows with vortex elements, Annual Reviews of Fluid Mechanics 17 (1985) 523–559.

[14] G.H. Markstein, Experimental and theoretical studies of flame-front stability, Journal of the Aeronautical Sciences 18 (1951) 199–209.

[15] V. Maz'ya, Approximate approximations, in: Proceedings of the Eighth Conference on the Mathematics of Finite Elements and Applications VIII, MAFELAP 1993, Brunel University, 1994, pp. 77–104.

[16] V. Maz'ya, G. Schmidt, On approximate approximations using Gaussian kernels, IMA Journal on Numerical Analysis 16 (1996) 13–29.

[17] V. Maz'ya, G. Schmidt, Construction of basis functions for high order approximate approximations, in: W.L. Wendland, M. Bonnet, A.-M. Sändig (Eds.), Mathematical Aspects of Boundary Element Methods, CRC Research Notes in Mathematics, Chapman & Hall, London, 1999, pp. 191–202.

[18] D.M. Michelson, G.I. Sivashinsky, Thermal-expansion induced cellular flames, Combustion and Flame 48 (1982) 211–217.

[19] Z. Olami, B. Galanti, O. Kupervasser, I. Procaccia, Random noise and pole dynamics in unstable front dynamics, Physical Review E 55 (3) (1997) 2649–2663.
[20] A.P. Prudnikov, Yu.A. Brichkov, O.I. Marichev, in: Integrals and Series, vol. 1, Nauka, Moscow, 1981.
[21] A.P. Prudnikov, Yu.A. Brichkov, O.I. Marichev, in: Integrals and Series, vol. 2, Gordon and Breach Science Publishers, New York, 1986.
[22] M. Rahibe, N. Aubry, G.I. Sivashinsky, Stability of pole solutions for planar propagating flames, Physical Review E 54 (5) (1996) 4958–4972.
[23] M. Rahibe, N. Aubry, G.I. Sivashinsky, Instability of pole solutions for planar propagating flames in sufficiently large domains, Combustion Theory and Modelling 2 (1) (1998) 19–41.
[24] G.I. Sivashinsky, Nonlinear analysis of hydrodynamic instability in laminar flames – I. Derivation of basic equations, Acta Astronautica 4 (1977) 1177–1206.
[25] G.I. Sivashinsky, Instabilities, pattern formation, and turbulence in flames, Annual Reviews of Fluid Mechanics 15 (1983) 179–199.
[26] O. Thual, U. Frisch, M. Hénon, Application of pole decomposition to an equation governing the dynamics of wrinkled flame fronts, Le Journal de Physique 46 (9) (1985) 1485–1494.
[27] L.N. Trefethen, Pseudospectra of linear operators, SIAM Review 39 (3) (1997) 383–406.
[28] C. Van Loan, Computational Frameworks for the Fast Fourier Transform, SIAM, Philadelphia, 1992.
[29] D. Vaynblat, M. Matalon, Stability of pole solutions for planar propagating flames: I. Exact eigenvalues and eigenfunctions, SIAM Journal on Applied Mathematics 60 (2) (2000) 679–702.